Vortex dynamics at high ac amplitudes of trifluoracetate route grown $YBa_2Cu_3O_{7-x}$-$BaZrO_3$ nanocomposites

E. Bartolomé,[1,2] A. Palau,[2] A. Llordés,[2] T. Puig,[2] and X. Obradors[2]
[1]*Escola Universitaria Salesiana de Sarrià, Passeig Sant Joan Bosco 74, 08017 Barcelona, Spain*
[2]*Institut de Ciència de Materials de Barcelona-CSIC, Campus UAB, 08193 Bellaterra, Spain*
(Received 2 December 2009; revised manuscript received 10 May 2010; published 27 May 2010)

$YBa_2Cu_3O_{7-x}$-$BaZrO_3$ (YBCO-BZO) nanocomposites have recently shown to display record pinning forces at high magnetic fields, paving thus the way for power applications. We have applied an ac-susceptibility methodology to analyze the different vortex dynamics of BZO nanocomposites compared to pristine YBCO thin films grown by the trifluoracetate route, close to the irreversibility line. The analysis is focused on the nonlinear Bean critical-state regime, occurring at high ac fields. We determined the dc-field and current-density dependencies of the effective energy barrier for thermally activated flux motion, $U_e(J,T,B)$. The distinctive dependencies encountered for BZO nanocomposites evidence that randomly oriented BZO nanoparticles in the YBCO matrix provide strong-isotropic pinning, even at very high dc fields and temperatures.

DOI: 10.1103/PhysRevB.81.184530 PACS number(s): 74.25.Ha, 74.72.−h

I. INTRODUCTION

In the quest to reach coated conductors with higher current performances, considerable effort has been made in the past years to enhance vortex pinning in YBCO through different nanoengineering strategies.[1–7] The chemical solution deposition method to grow $YBa_2Cu_3O_{7-x}$ (YBCO) based on triofluoracetate (TFA) precursors is probably the most promising route toward the manufacturing of low-cost, kilometer-long coated conductors. Recently, TFA-YBCO thin films with record pinning forces (22 GN/m^3 at 77 K and 2 T and 78 GN/m^3 at 65 K and 3 T) have been achieved by addition of $BaZrO_3$ (BZO) nanoparticles into the YBCO matrix.[5] This represents an increase of a factor 12 from the standard values of TFA-YBCO thin films. The origin of this enhanced performance has been correlated with an increase in the microstrain, induced by the randomly oriented BZO nanodots.[8] Static pinning phase diagrams in the (H_{dc},T) plane obtained using a transport methodology showed that BZO nanocomposites induced an isotropic-strong pinning contribution dominating most of the phase diagram.[9] In contrast, for standard TFA-YBCO films, different regions of prevalence of isotropic-weak, isotropic-strong, and anisotropic pinning could be distinguished.

An important question still to be solved is how BZO nanoparticles affect pinning at very high magnetic fields and temperatures, close to the irreversibility line (IL). ac susceptibility has proven in the past to be one of the best techniques to investigate vortex dynamic issues close to the IL.[10] Campbell and Evetts[11] early works, followed by others,[12] settled down the theoretical basis for the analysis of the ac response in vortex matter. They described the existence of a linear, Campbell regime at low ac fields, arising from the oscillation of pinned vortices inside pinning potential wells, crossing over to a nonlinear regime at intermediate ac fields. At high enough ac amplitudes, a Bean critical state develops. Pasquini *et al.*[13] proposed a methodology to determine the vortex phase diagram in the (H_{ac},T) plane including the different ac regimes. This technique was used in the past to analyze the vortex dynamics of as-grown and ion-irradiated YBCO thick films,[13] pulsed laser deposition (PLD)-grown YBCO epitaxial thin films, and coated conductors.[14]

In this work, we have investigated by ac susceptibility the vortex dynamics of BZO nanocomposites and standard YBCO thin films grown by the TFA route, to understand the pinning introduced by the different kinds of nanodefects close to the IL. We have focused on the description of the ac response in the critical-state regime at high ac fields. In particular, we have determined the activation energy for depinning, U_e, which is the height of the potential barrier that vortices must overcome when hopping from a pinning site to another. The temperature, dc magnetic field, and current-density dependence of the energy for thermally activated vortex motion, $U_e(T,H_{dc},J)$, for standard $YBCO^{TFA}$ thin films and BZO nanocomposites is obtained. Results show that BZO nanocomposites present distinctive dependencies compared to as-grown thin films, which may be ascribed to the presence of randomly oriented nanodots providing strong-isotropic pinning.

II. SAMPLES AND EXPERIMENTAL DETAILS

Epitaxial *c*-axis-oriented YBCO- and BZO-nanocomposite thin films were grown on single-crystalline $LaAlO_3$ and $SrTiO_3$ substrates. Samples were prepared from metal-organic precursor solutions with stoichiometric quantities of Y, Ba, and Cu anhydrous TFA, with the addition of Ba trifluoroacetate and Zr acetylacetonate.[15–17] After spinning of the solution on the substrate, samples were pyrolyzed following a short process (<2 h) (Ref. 18) in which samples were heated up to 310 °C. Films were grown during 150 min at a reacting temperature (between 810 and 840 °C) in a wet, $P(H_2O)=22$ mbar, nitrogen atmosphere with a partial oxygen pressure of 0.2 mbar. Finally, the superconducting phase was achieved by oxygen annealing at 450 °C.

Standard $YBCO^{TFA}$ films grown by this procedure contain both defects along the *ab* direction (Cu-O planes, stacking faults, intergrowths[19,20]) and in the *c* direction (threading dislocations, twin boundaries, etc.[21–23]).

The addition of BZO precursors to the initial solution leads to the formation of YBCO epitaxial films with two nanoparticle populations: epitaxial particles nucleated at the substrate-precursor interface, and a major population of noncoherent BZO particles randomly distributed in the YBCO matrix.[5] Indeed, inspection of the typical x-ray diffraction pattern of a BZO nanocomposite shows the presence of expected phases with *c*-preferred orientation, evidenced by the (00ℓ) diffraction spots and, additionally, a randomly oriented BZO fraction, evidenced from the diffraction ring at $2\theta \sim 30°$, which accounts for the (110)-BZO maximum intense line [Fig. 1(a)].

The pole figure of the (104)/(014) diffracting plane of YBCO in BZO nanocomposites demonstrates the biaxial texture is maintained [Fig. 1(b)]. Moreover, the in-plane and out-of-plane misorientation spread does not vary significantly in the nanocomposites. $\Delta\Phi$ values ranging from 1.2° to 1.3° and $\Delta\omega$ from 0.5° to 0.6° were obtained in all studied samples.

BZO coherent domain sizes (along *c*-axis direction) were estimated from the integral breadth of the BZO line (200) by using the Scherrer formula, $D=0.9\lambda/\beta\cos\theta$,[24] where λ is the x-ray wavelength. This expression relates the integral breadth (β) of a given peak in the 2θ scan with the apparent domain size D along the diffracting plane normal. In order to not overestimate the domain size, the instrumental broadening was subtracted. Sizes between ~10–20 nm were obtained for the concentration range tested (4–20 mol % BZO). These results are in agreement with nanoparticle dimensions determined from transmission electron microscope (TEM) images, already reported in Ref. 5, where it was also shown that epitaxial and random particles had similar sizes.

For this work, we considered three $YBCO^{TFA}$ films (A, B, and C) with typical critical current densities ($J_c = 4-6$ MA/cm^2 in self-field at 77 K), and three BZO nanocomposites with different BZO molar concentration (7%, 10%, and 13%). The critical temperature, determined from electrical resistivity, was $T_c \sim 91.5$ K for all samples, independent of the BZO content. All studied samples had the same dimensions (5×5 mm^2), and film thickness (250 nm).

ac-susceptibility measurements as a function of temperature were performed with a Quantum Design PPMS (physical property measurement system), at driving ac amplitudes between $\mu_0 H_{ac}=0.01-1.5$ mT applied perpendicular to the substrate. The frequency and dc field were varied, respectively, between $f=11-1111$ Hz and 0–9 T. Transport experiments were performed with the current injected parallel to the *ab* planes, in 0–9 T magnetic fields applied perpendicular to the substrate.

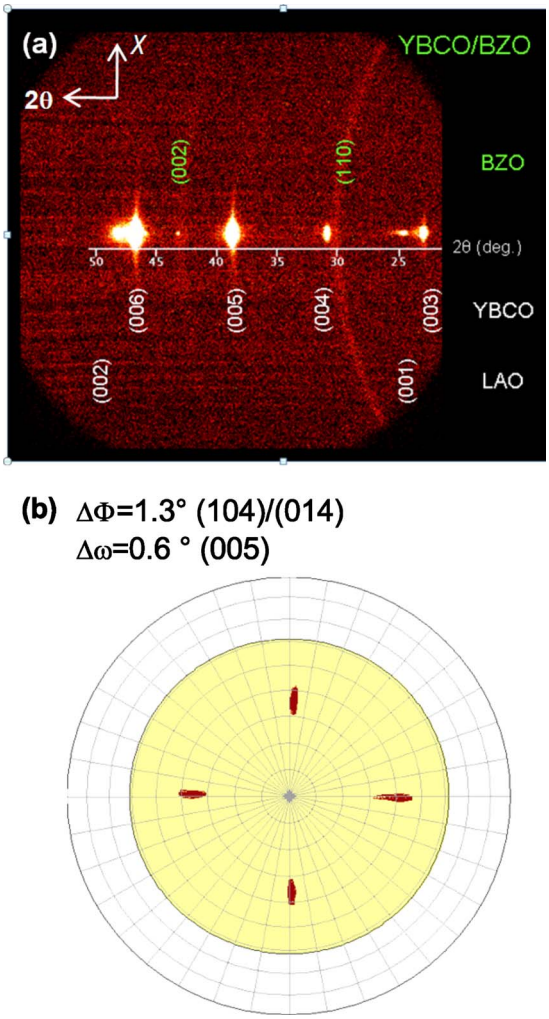

FIG. 1. (Color online) Structural characterization of an YBCO/BZO nanocomposite with 10 mol % of BZO; (a) x-ray diffraction pattern in two dimensions $(2\theta,\chi)$ obtained with a general area diffraction system from Brucker. The diffraction spots of the BZO and YBCO phases are identified. Note the coexistence of diffracted intensities for BZO corresponding to textured and randomly oriented nanoparticles; (b) pole figure of the (104)/(014) diffracting plane of YBCO. The main four poles located at a tilt angle of $\chi \sim 37°$ demonstrate the biaxial texture of the film since for a perfectly *c*-oriented film this reflection only appears at such tilting. In addition, the sole presence of four peaks, 90° apart by crystal symmetry, denotes a unique in-plane orientation. In-plane and out-of-plane misorientation values of $\Delta\Phi \sim 1.3°$ and $\Delta\omega \sim 0.6°$ were obtained for this nanocomposite.

III. ac-SUSCEPTIBILITY RESULTS

The objective of our work was the analysis of the ac response of standard $YBCO^{TFA}$ thin films and BZO nanocomposites, specifically in the Bean critical-state regime. Therefore, we first experimentally determined the onset of the Bean state for both kinds of films (Sec. III A). Then, ac measurements were carried out at fixed ac amplitude, above the Bean onset line. Section III B presents results on the activation energy in the Bean regime for the two different kinds of films.

A. Onset of Bean critical-state regime

We applied the methodology proposed by Pasquini *et al.*[13] to determine the position of the Bean onset line $H_{ac}^{c}(T)$ within the general (H_{ac},T) vortex dynamic phase diagram. Since the position of the $H_{ac}^{c}(T)$ line increases with the dc field, we chose to determine it at the smallest possible dc magnetic field (self-field, $\mu_0 H_{dc} \sim 5$ mT), in order to guar-

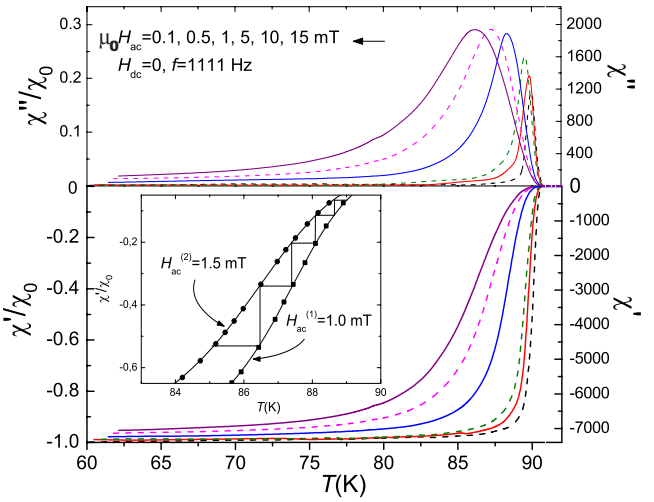

FIG. 2. (Color online) Temperature dependence of the real, χ', and the imaginary, χ'', components of the ac susceptibility, and the values normalized to its Meissner slope, χ'/χ_0 and χ''/χ_0 for ac fields $\mu_0 H_{ac}$=0.01, 0.05, 0.1, 0.5, 1, and 1.5 mT at 1111 Hz and self-field (5 mT) for the standard YBCO^{TFA} thin film. Inset. Determination of the Bean length from the χ'/χ_0 data through method described by Pasquini *et al.* (Ref. 13).

antee that activation energy measurements at higher dc fields (Sec. III B) would always fall within the Bean regime.

We measured the temperature dependence of the normalized real and the imaginary components of the ac susceptibility (normalized to the Meissner slope), χ'/χ_0 and χ''/χ_0, at different ac-field amplitudes $\mu_0 H_{ac}$, constant frequency f =1111 Hz, and self-field, Fig. 2.

At sufficiently high ac amplitudes, vortices perform large excursions outside the pinning wells and the ac response is well described by the Bean critical state. In this regime, the persistent current density is uniform, as determined by the balance between Lorentz and pinning forces. Then, since J_c is independent of H_{ac}, the characteristic Bean length,

$$\Lambda_c = H_{ac}/J_c(T) \tag{1}$$

is proportional to H_{ac}. The $\Lambda_c(\chi'/\chi_0')$ is experimentally determined according to Ref. 13 from two $\chi'/\chi_0(T)$ curves at $\mu_0 H_{ac}^{(1)}$=1.0 mT and $\mu_0 H_{ac}^{(2)}$=1.5 mT, that are presumed high enough to be in the critical regime. The method consists of generating the function $\chi'/\chi_0=\gamma^n[\Lambda_c]_A$, where $\gamma=H_{ac}^{(2)}/H_{ac}^{(1)}$ and n is the index of the n-sim ladder step in Fig. 2, inset. The curve is then well defined as a function of a $[\Lambda_c]_A$ factor, which can be fixed assuming a particular geometrical model. We obtained the absolute values of Λ_c from Eq. (1), considering the thin-film disk approximation, where the critical current density is $J_c(T_{peak})=2H_{ac}/1.94t$, and that χ'/χ_0 at the χ'' peak position T_{peak} is $\chi'/\chi_0=-0.38$ in the Bean regime.[25]

From the $\Lambda_c(\chi'/\chi_0)$ plot [Fig. 3(a)] and using the $\chi'/\chi_0(T)$ curves presented in Fig. 2, we determine the Bean length as a function of H_{ac} for a series of different temperatures [Fig. 3(b)]. The onset of the Bean regime, $H_{ac}^c(T)$, is determined from the deviation of $\Lambda_c(H_{ac})$ to the linearity.

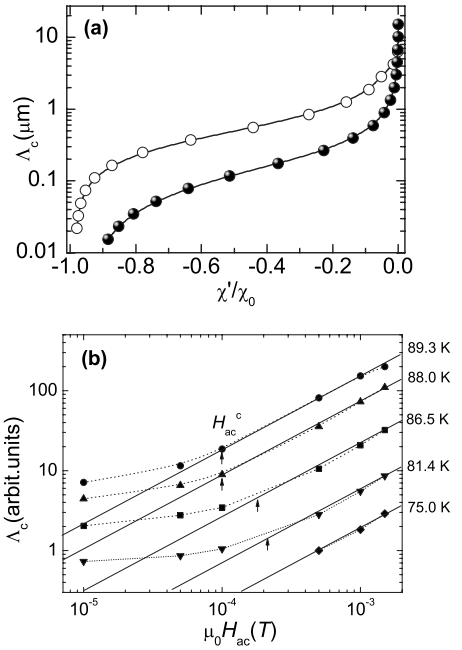

FIG. 3. (a) Bean length, Δ_c, as a function of χ'/χ_0 obtained through the method described by Pasquini *et al.* (Ref. 13) for standard YBCO^{TFA} thin film A (○) and 7% BZO nanocomposite (●); (b) determination of the Bean onset, $H_{ac}^c(T)$, from the deviation of the Bean length $\Delta_c(H_{ac},T)$ from linearity, shown as example for standard YBCO^{TFA} film A.

Figure 4 shows the Bean $H_{ac}^c(T)$ line for several standard YBCO^{TFA} films and BZO nanocomposites of different concentration. It can be observed that the $H_{ac}^c(T)$ line is very similar for all the samples studied within the experimental error. A similar effect was observed in the vortex phase diagram of PLD-YBCO thin films and coated conductors,[14] where the different kinds of defects produced a change on the nonlinear onset curve, $H_{ac}^1(T)$, but did not influence the $H_{ac}^c(T)$ line. This result indicates that at very large ac fields, the driving oscillations are much larger than the details of the pinning potential washboard; hence the critical state is estab-

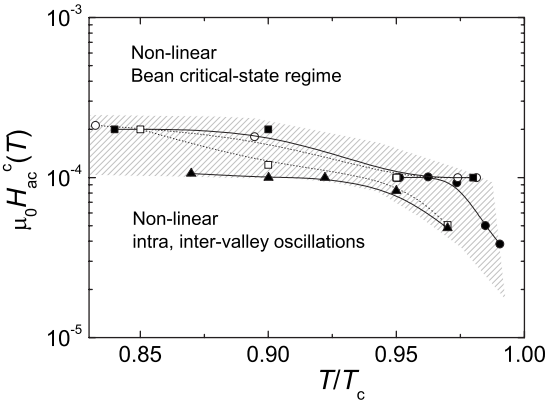

FIG. 4. Bean regime onset lines $H_{ac}^c(T/T_c)$ within the (H_{ac},T) dynamic phase diagrams in self-field, f=1111 Hz, for standard YBCO^{TFA} samples (○ A and □ B), and BZO nanocomposites with different concentration: 7% (▲), 10% (●), and 13% (■). The data error bars are between 0.5×10^{-4}–1×10^{-4} T.

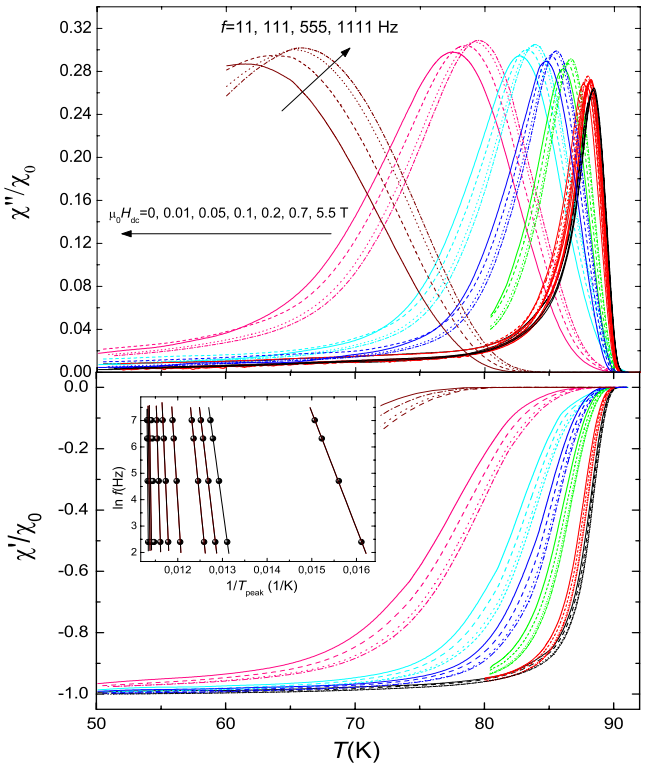

FIG. 5. (Color online) Temperature dependence of the normalized real and imaginary susceptibilities, χ'/χ_0 and χ''/χ_0, at $\mu_0 H_{ac}=0.5$ mT, for dc fields $\mu_0 H_{dc}=0$, (0.005), 0.01, (0.02), 0.05, 0.1, 0.2, (0.5), 0.7, (1.2), 5.5 T (raw data at fields between brackets have been omitted for the sake of clarity), each at frequencies $f=11$, 111, 555, and 1111 Hz (from left to right). Inset. Arrhenius plot, $\ln(f)$ versus $1/T_{peak}$ for the above dc fields (standard YBCO^{TFA} sample A).

lished as a result of a global motion of all vortices in the sample at similar ac-field amplitudes.

B. Activation energy in Bean critical-state regime

ac-susceptibility measurements of high T_c superconductors have revealed the importance of the frequency dependence in the determination of the critical current density due to the strong influence of flux creep. For thermally activated vortex motion, the shift in the temperature of maximum losses (T_{peak}) with the frequency can be described in terms of an Arrhenius law,[10]

$$f = f_0 \exp[U_e(B)/kT_{peak}], \tag{2}$$

where f_0 is the characteristic attempt frequency for vortex hopping and k is the Boltzmann constant. In general, the activation energy can be factorized as[13,26–28]

$$U_e(T,H_{dc},J) = U_e(T)U_e(H_{dc})U_e(J). \tag{3}$$

In order to study the field dependence of the activation energy, we have analyzed the shift of the $\chi''(T)$ peak at T_{peak} as a function of frequency, at different applied dc fields (Fig. 5). Measurements were done at an ac field of 0.5 mT so as to work above the previously determined $\mu_0 H_{ac}^c(T)$ Bean onset

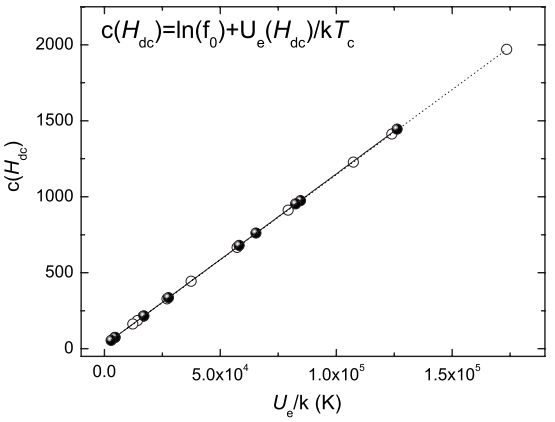

FIG. 6. Constant term in the Arrhenius linear fits (Fig. 5, inset) as a function of the activation energy, for a standard YBCO^{TFA} sample A (○) and a 7% BZO nanocomposite (●).

line within the phase diagram. Figure 5 inset shows the Arrhenius plots $\ln(f)$ versus $1/T_{peak}$, obtained at several applied dc magnetic fields.

As shown in Fig. 6, the constant terms of the Arrhenius fits, $c(H_{dc})$, are linearly dependent on the activation energy, $U_e(H_{dc})$. As extensively discussed in Ref. 28, this implies that the temperature dependence of the effective energy barriers can be assumed to be linear, i.e., $U_e(H_{dc},T) = U_e(H_{dc})(1-T/T_c)$. In that case, the constant term $c(H_{dc})$ can be then written as $c(H_{dc})=\ln(f_0)+U_e(H_{dc})/kT_c$, and f_0 and T_c can be determined by fitting the $c(U_e)$ data. For the standard film and BZO nanocomposite, we have obtained the attempt frequencies $f_0=8\times10^{10}$ Hz and $f_0=2\times10^{10}$ Hz, and critical temperatures $T_c=89.3$ K and $T_c=88.7$ K, respectively.

We have determined the activation energy at each H_{dc} by using [Eq. (2)]. Figure 7 plots for comparison the obtained dc magnetic field dependence of the activation energy for an as-grown YBCO^{TFA} thin film and a BZO nanocomposite. It can be clearly observed that the two kinds of samples exhibit very different $U_e(H_{dc})$ dependencies:

The standard YBCO^{TFA} thin film presents a plateau at low dc magnetic fields and a power-law dependence $U_e(H_{dc}) \propto (H_{dc}/H_0)^{-\beta}$, with $\beta\sim0.5$ at high magnetic fields. The plateau is associated with a single-vortex pinning regime whereas the power-law exponent at high magnetic fields is similar to values observed for thermally activated plastic motion[29] or for flux pinning controlled by planar defects.[30,31] The latter would indicate that flux pinning is dominated by twin planes, in agreement with the high density of twins observed in YBCO thin films.[21,32,33] A clearly defined crossover field $\mu_0 H_{cross}$, marks the transition from the single-vortex pinning regime to the regime dominated by vortex-vortex interaction.

In contrast, the $U_e(H_{dc})$ dependence of all BZO nanocomposites presented a much smoother behavior, impossible to be fitted by a power law. The values of the activation energies in self-field, $U_e(0)$, had typical values around 10^5 K, similar to other published YBCO thin films,[14,34] with sample to sample variations between $0.9\times10^5-2.5\times10^5$ K. The normalized $U_e/U_e(0)$ dependence on the dc field of all BZO

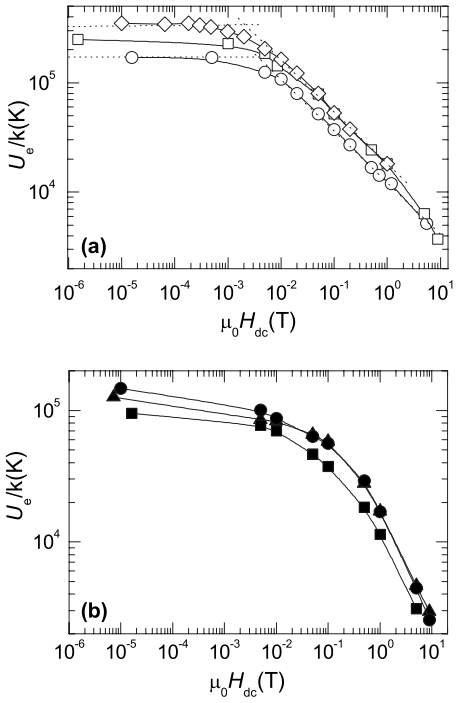

FIG. 7. Field dependence of the activation energy, $U_e(H_{dc})$, for (a) standard YBCO^{TFA} samples A (○), B (□), and C(◇); (b) BZO nanocomposites with different concentration: 7% (▲), 10% (●), and 13% (■).

nanocomposites presented a distinctive, rounded behavior compared to the as-grown films, indicating a different vortex-pinning regime mediated by vortex-vortex interaction (Fig. 8). The activation energy at high dc fields was always larger than that of pristine samples. This would be in agreement with the extremely high pinning forces measured for these samples at high dc fields.[5]

It should be noted also that critical current-density field dependencies, $J_c(H_{dc})$, obtained from transport in self-field at a fixed temperature (77 K) of BZO nanocomposites presented also a smoother aspect, compared to YBCO^{TFA} thin

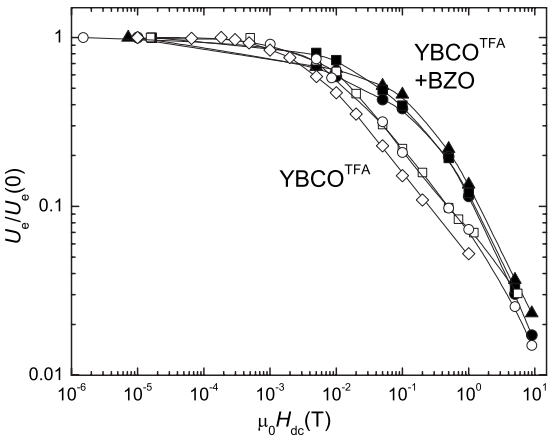

FIG. 8. Field dependence of the normalized activation energy, $U_e(H_{dc})/U_e(0)$, for standard YBCO^{TFA} samples A (○), B (□), and C(◇) and BZO nanocomposites with different molar concentration: 7% (▲), 10% (●), and 13% (■).

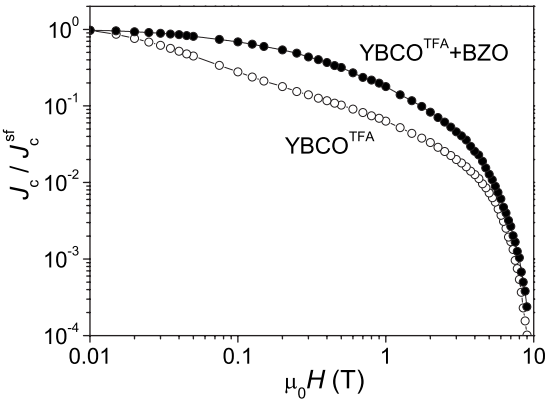

FIG. 9. Field dependence of the critical current density normalized by the value in self-field, J_c/J_c^{sf}, at 77 K for a standard YBCO^{TFA} sample A (○) with J_c^{sf}=4.5 MA/cm^2, and a 7% BZO nanocomposite (●) with J_c^{sf}=5.4 MA/cm^2.

films (Fig. 9). Standard films displayed a typical plateau and a power-law dependence $J_c/J(0)=(H/H_0)^{-\alpha}$, with α=0.5 corresponding respectively to the single-vortex and vortex-vortex interaction regimes whereas BZO nanocomposites present a rounded $J_c(H_{dc})$ dependence. This evidences that the presence of BZO random nanodots significantly changes the dc-field dependence in very different regions of the (H,T) diagram.

We turn our attention now to the current-density dependence of the activation energy. $U_e(J)$ was determined from the analysis of the frequency dependence of the temperature at a fixed value of χ' proportional to J. The $U_e(\chi')$ function was obtained by fitting the Arrhenius plots ln(f) vs $1/T$ at different χ'. Then, the $\chi'(J)$ dependence was determined using Eq. (1) and the $\Lambda_c(\chi'/\chi_0)$ with defined units shown in Fig. 3.

Note that $U_e(H_{dc},J)$ was independently analyzed as $U_e(H_{dc})U_e(J)$. In order to validate this approach, several $U_e(J)$ were determined at different H_{dc} [Fig. 10(a)]. By using the $U_e(H_{dc})$ dependence found for each film, we could collapse all the $U_e(J)$ curves [Fig. 10(b)], confirming that the $U_e(H_{dc},J)$ dependence could be indeed factorized in two independent terms. The $U_e(J)$ curves of standard YBCO^{TFA} films and BZO nanocomposites are again quite different (Fig. 10).

The $U_e(J)$ of the standard YBCO^{TFA} sample displays two well-differentiated dependencies. As shown in Fig. 11, at low current densities the curve can be fitted by Feigelman-Blatter expression,[35]

$$U_e(J) = U_c\left(\frac{J_c}{J}\right)^{\mu} \tag{4}$$

with a small μ=0.2 exponent (tending to a logarithmic trend reported by others[33,36,37]), which can correspond to a vortex pinning dominated by planar, anisotropic defects.[37] At high current densities, the curve can be fitted with a μ=0.74 exponent, similar to that predicted for a collective flux creep regime caused for large vortex bundles μ=7/9.[30] A similar behavior has been described for PLD-grown YBCO thin

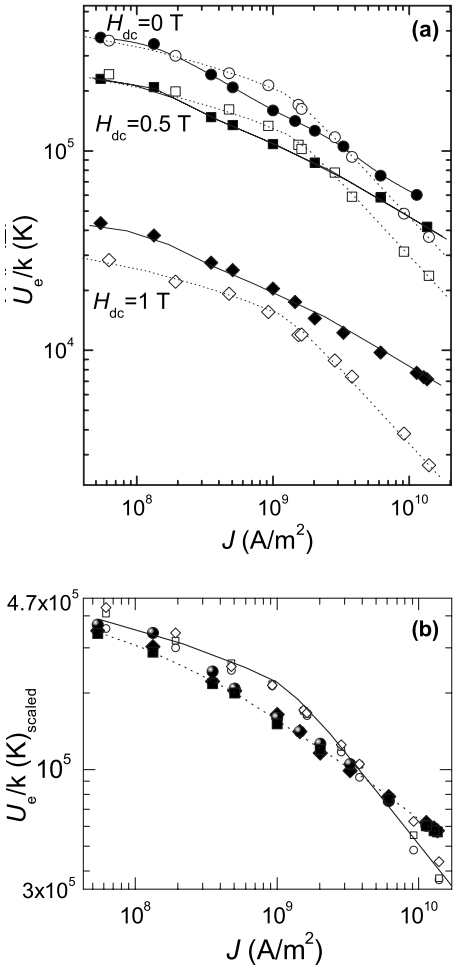

FIG. 10. (a) Activation energy vs current density for the standard YBCO^{TFA} sample A (open symbols) and a 7% BZO nanocomposite (closed symbols), at $\mu_0 H_{ac}$=5 mT and dc fields $\mu_0 H_{dc}$=0 (circles), 0.5 T (squares), and 1 T (rhomboids); (b) U_e/k(H_{dc}) curves scaled according to the $U_e(H_{dc})$ dependence shown in Fig. 7. Lines are guide for the eyes.

films, coated conductors,[14] and melt-powder-melt-growth YBCO.[30]

In contrast, the $U_e(J)$ curve of the BZO nanocomposite presents a smoother J decay, which can be fitted with μ =0.4. In this case, a single dynamic behavior is observed up to the highest current densities scanned (J=10^{10} A/m^2). We suggest that this dependence may be ascribed to the isotropic-strong pinning induced by the extended BZO defects. It should be noted that a theoretical prediction of $U_e(J)$ for this kind of pinning is not available.

Summarizing, it has been found that the activation energy dependence with the temperature, applied dc magnetic field, and current density for YBCO^{TFA} films can be described by

$$U_e(T,H_{dc},J) = U_0\left[1-\left(\frac{T}{T_c}\right)\right]\left(\frac{H_{dc}}{H_0}\right)^{-\beta}\left(\frac{J}{J_0}\right)^{-\mu}, \qquad (5)$$

where, U_0, H_0, and J_0 are scaling values, β=0,0.5 (for H $<H_0$ and $H>H_0$, respectively) and μ=0.2,0.74 (for $J<J_0$ and $J>J_0$, respectively).

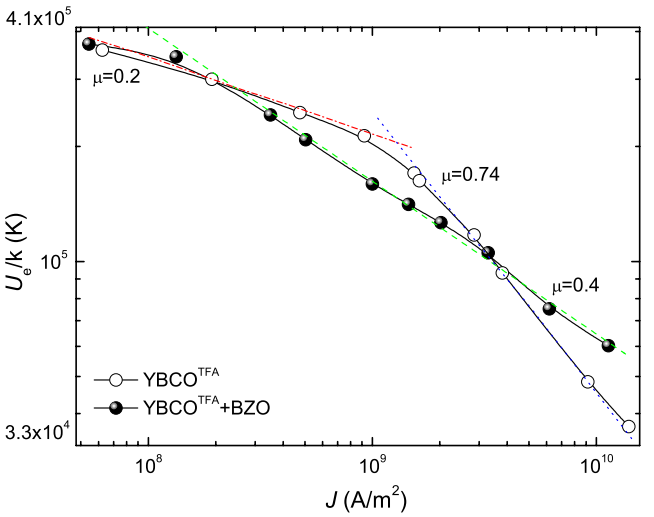

FIG. 11. (Color online) Fitting of the activation energy vs current density at $\mu_0 H_{ac}$=5 mT and self-dc field for a standard YBCO^{TFA} sample, A (○), and a 7% BZO nanocomposite (●), using Feigelman-Blatter expression, Eq. (4).

For BZO nanocomposites, the activation energy can be also factorized in three separate terms,

$$U_e(T,H_{dc},J) = U_0\left[1-\left(\frac{T}{T_c}\right)\right]f(H_{dc}/H_0)\left(\frac{J}{J_0}\right)^{-\mu}, \qquad (6)$$

where μ=0.2,0.4 (for $J<J_0$ and $J>J_0$, respectively). However, different from standard films, the dc-field dependence is a function, $f(H_{dc}/H_0)$, that cannot be expressed as a power law.

IV. DISCUSSION

The above experimental results evidence that YBCO^{TFA} thin films including BZO nanoparticles display distinctive $U_e(H_{dc})$ and $U_e(J)$ dependencies compared to as-grown samples.

We believe the origin of this behavior may rely on the presence of the randomly oriented BZO nanoinclusions in the YBCO matrix. T. Puig *et al.*[9] showed that standard and BZO nanocomposites have very different (static) pinning phase diagrams. Close to the IL, defects present in standard TFA thin films give a major anisotropic pinning contribution (80%) whereas the isotropic-strong contribution is small (20%) and the isotropic-weak is nonexistent. In contrast, BZO random nanoparticles produce mainly (80–90 %) isotropic-strong pinning whereas the anisotropic contribution is just 20–10 %, and there is no isotropic-weak pinning. Thus, this suggests that the addition of a major isotropic-strong pinning contribution induced by the BZO nanocomposites to the preexisting anisotropic pinning gives rise to characteristic rounded $U_e(H_{dc},J)$ curves, different from those associated solely to correlated defects.

The experimental data found for BZO nanocomposites cannot be described by any of the theoretical pinning models available at present. Indeed, the weak-collective theory developed by Larkin-Ovchinnikob[38] is applicable to pointlike

weak defects whereas BZO induce strong, extended defects. van der Beek *et al.*[39] developed a theory for sparse large point pins (such as Y_2O_3 inclusions) by substitution of the elementary pinning force of a large void into the collective pinning expression, and derived expressions for the critical current-density field dependence in different field ranges, however explicit expressions for the activation energy seem not straightforward to obtain. Strong-pinning theories[35,40] have been developed to describe anisotropic pinning produced by columnar heavy-ion irradiation defects or planar defects[41] such as twin boundaries. In future, an effort should be done to develop a full theoretical frame able to explain the observed experimental phenomena associated to extended isotropic-strong pinning defects.

V. CONCLUSIONS

ac-susceptibility analysis represents an attractive approach for studying the correlation between the pinning and differently nanoengineered YBCO thin films, at the region close to the IL. This is important toward controlling and enhancing current properties by nanodefect tailoring.

The ac-susceptibility technique has been used to analyze and compare the vortex pinning and dynamic response of TFA-grown epitaxial YBCO thin films and BZO nanocomposites. We focused on the study of the ac response in the nonlinear Bean regime at high ac fields, above the onset $H_{ac}^{c}(T)$ line. We determined the explicit factorization of the effective energy barrier for flux motion activated thermally, as a function of the dc applied field, the temperature, and the current density, $U_e(H_{dc},T,J)$, for both kinds of films. Results show that the $U_e(H_{dc})$ and $U_e(J)$ dependencies of BZO nanocomposites present distinctive, rounded dependencies compared to as-grown $YBCO^{TFA}$ thin films. The origin of these particularly rounded curves, never reported before, may be ascribed to the presence of randomly oriented nanodots, which provide an strong-isotropic pinning contribution close to the IL, instead of the major anisotropic pinning induced by other kinds of nanodefects.

ACKNOWLEDGMENTS

We acknowledge the financial support from MICINN (Grants No. MAT2008-01022, No. NAN2004-09133-CO3-01, and Consolider NANOSELECT), Generalitat de Catalunya (Catalan Pla de Recerca 2009-SGR-770 and XaRMAE), and EU (HIPERCHEM and NESPA).

[1] J. L. MacManus-Driscoll, S. R. Foltyn, Q. X. Jia, H. Wang, A. Serguis, L. Civale, B. Maiorov, M. E. Hawley, M. P. Maley, and D. E. Peterson, Nature Mater. **3**, 439 (2004).

[2] A. Goyal, S. Kang, K. J. Leonard, P. M. Martin, A. A. Gapud, M. Varela, M. Paranthaman, A. O. Ijaduola, E. D. Spetch, J. R. Thompson, D. K. Christen, S. J. Pennycook, and F. A. List, Supercond. Sci. Technol. **18**, 1533 (2005).

[3] Y. Yamada, K. Takahashi, H. Kobayashi, M. Konishi, T. Watanabe, A. Ibi, T. Muroga, S. Miyata, T. Kato, T. Hirayama, and Y. Shiohara, Appl. Phys. Lett. **87**, 132502 (2005).

[4] P. Mele, K. Matsumoto, T. Horide, O. Miura, A. Ichinose, M. Mukaida, Y. Yoshida, and S. Horii, Supercond. Sci. Technol. **19**, 44 (2006).

[5] J. Gutiérrez, A. Llordés, J. Gázquez, M. Gibert, N. Romà, S. Ricart, A. Pomar, F. Sandiumenge, N. Mestres, T. Puig, and X. Obradors, Nature Mater. **6**, 367 (2007).

[6] T. G. Holesinger, L. Civale, B. Maiorov, D. M. Feldmann, J. Y. Coulter, J. Miller, V. A. Maroni, Z. J. Chen, D. C. Larbalestier, R. Feenstra, X. P. Li, M. B. Huang, T. Kodenkandath, W. Zhang, M. W. Rupich, and A. P. Malozemoff, Adv. Mater. **20**, 391 (2008).

[7] B. Maiorov, S. A. Baily, H. Zhou, O. Ugurlu, J. A. Kennison, P. C. Dowden, T. G. Holesinger, S. R. Foltyn, and L. Civale, Nature Mater. **8**, 398 (2009).

[8] A. Pomar, V. R. Vlad, A. Llordés, A. Palau, J. Gutiérrez, S. Ricart, T. Puig, X. Obradors, and A. Usoskin, IEEE Trans. Appl. Supercond. **19**, 3258 (2009).

[9] T. Puig, J. Gutiérrez, A. Pomar, A. Llordés, J. Gázquez, S. Ricart, F. Sandiumenge, and X. Obradors, Supercond. Sci. Technol. **21**, 034008 (2008).

[10] F. Gömöry, Supercond. Sci. Technol. **10**, 523 (1997).

[11] A. M. Campbell, J. Phys. C **4**, 3186 (1971); A. M. Campbell and J. E. Evetts, Adv. Phys. **21**, 199 (1972).

[12] C. J. van der Beek, V. B. Geshkenbein, and V. M. Vinokur, Phys. Rev. B **48**, 3393 (1993).

[13] G. Pasquini, L. Civale, H. Lanza, and G. Nieva, Phys. Rev. B **59**, 9627 (1999).

[14] A. Palau, T. Puig, and X. Obradors, J. Appl. Phys. **102**, 073911 (2007).

[15] X. Obradors, T. Puig, A. Pomar, F. Sandiumenge, N. Mestres, M. Coll, A. Cavallaro, N. Roma, J. Gázquez, J. C. González, O. Castaño, J. Gutiérrez, A. Palau, K. Zalamova, S. Morlens, A. Hassini, M. Gibert, S. Ricart, J. M. Moreto, S. Piñol, D. Isfort, and J. Bock, Supercond. Sci. Technol. **19**, S13 (2006).

[16] T. Puig, J. C. González, A. Pomar, N. Mestres, O. Castaño, M. Coll, J. Gázquez, F. Sandiumenge, S. Piñol, and X. Obradors, Supercond. Sci. Technol. **18**, 1141 (2005).

[17] N. Roma, S. Morlens, S. Ricart, K. Zalamova, J. M. Moreto, A. Pomar, T. Puig, and X. Obradors, Supercond. Sci. Technol. **19**, 521 (2006).

[18] K. Zalamova, N. Roma, A. Pomar, S. Morlens, T. Puig, J. Gazquez, A. E. Carrillo, F. Sandiumenge, S. Ricart, N. Mestres, and X. Obradors, Chem. Mater. **18**, 5897 (2006).

[19] L. Civale, B. Maiorov, J. L. Manus-Driscoll, H. Wang, T. G. Holesinger, S. R. Foltyn, A. Serquis, and R. N. Arendt, IEEE Trans. Appl. Supercond. **15**, 2808 (2005).

[20] S. I. Kim, A. Gurevich, X. Song, X. Li, W. Zhang, T. Kodenkandath, M. W. Rupich, T. G. Holesinger, and C. Larbalestier, Supercond. Sci. Technol. **19**, 968 (2006).

[21] A. Palau, J. H. Durrell, J. L. MacManus-Driscoll, S. Harrington, T. Puig, F. Sandiumenge, X. Obradors, and M. G. Blamire, Phys. Rev. Lett. **97**, 257002 (2006).

[22] A. Díaz, L. Mechin, P. Berghuis, and J. E. Evetts, Phys. Rev. Lett. **80**, 3855 (1998).
[23] L. Civale, B. Maiorov, A. Serquis, J. O. Willis, J. Y. Coulter, H. Wang, Q. X. Jia, P. N. Arendt, J. L. MacManus-Driscoll, M. P. Maley, and S. R. Foltyn, Appl. Phys. Lett. **84**, 2121 (2004).
[24] P. Scherrer, Göttinger Nachrichten Gesell. **2**, 98 (1918).
[25] J. R. Clem and A. Sánchez, Phys. Rev. B **50**, 9355 (1994).
[26] P. J. Kung, M. P. Maley, M. E. Mchenry, J. O. Willis, J. Y. Coulter, M. Murakami, and S. Tanaka, Phys. Rev. B **46**, 6427 (1992).
[27] M. J. Qin, X. Jin, H. L. Ji, Z. X. Shi, X. X. Yao, Z. G. Fan, and Y. Q. Shan, J. Appl. Phys. **77**, 2618 (1995).
[28] L. Fàbrega, J. Fontcuberta, S. Piñol, C. J. van der Beek, and P. H. Kes, Phys. Rev. B **47**, 15250 (1993); L. Fàbrega, J. Fontcuberta, L. Civale, and S. Piñol, *ibid.* **50**, 1199 (1994).
[29] V. M. Vinokur, M. V. Feigelman, V. B. Geshkenbein, and A. I. Larkin, Phys. Rev. Lett. **65**, 259 (1990).
[30] P. J. Kung, M. P. Maley, M. E. Mchenry, J. O. Willis, M. Murakami, and S. Tanaka, Phys. Rev. B **48**, 13922 (1993).
[31] T. Matsushita, S. Funaba, Y. Nagamatsu, B. Ni, K. Funaki, and K. Yamafuji, Jpn. J. Appl. Phys., Part 2 **28**, L1508 (1989).
[32] J. M. Huijbregtse, F. C. Klaassen, A. Szepielow, J. H. Rector, B. Dam, R. Griessen, B. J. Kool, and J. T. M. de Hosson, Supercond. Sci. Technol. **15**, 395 (2002).
[33] E. Zeldov, N. M. Amer, G. Koren, A. Gupta, and M. W. McElfresh, Appl. Phys. Lett. **56**, 680 (1990).
[34] X. Xiaojun, F. Lan, W. Liangbin, Z. Yuheng, F. Jun, C. Xiaowen, L. Kebin, and S. Hisashi, Phys. Rev. B **59**, 608 (1999).
[35] G. Blatter, M. V. Feigel'man, V. B. Geshkenbein, A. I. Larkin, and V. M. Vinokur, Rev. Mod. Phys. **66**, 1125 (1994).
[36] J. Li, S. Y. Ding, J. S. Zhu, H. M. Shao, and Y. N. Wang, J. Appl. Phys. **77**, 6398 (1995).
[37] M. J. Qin, S. Y. Ding, C. Ren, X. X. Yao, Y. X. Fu, C. B. Cai, T. S. Shi, and G. Y. Wang, Physica C **262**, 127 (1996).
[38] A. I. Larkin and Yu. N. Ovchinnikov, Zh. Eksp. Teor. Fiz. **65**, 1704 (1973); J. Low Temp. Phys. **34**, 409 (1979).
[39] C. J. van der Beek, M. Konczykowski, A. Abal'oshev, I. Abal'osheva, P. Gierlowski, S. J. Lewandowski, M. V. Indenbom, and S. Barbanera, Phys. Rev. B **66**, 024523 (2002).
[40] F. C. Klaassen, G. Doornbos, J. M. Huijbregtse, R. C. F. van der Geest, B. Dam, and R. Griessen, Phys. Rev. B **64**, 184523 (2001).
[41] A. Petković, T. Emig, and T. Nattermann, Phys. Rev. B **79**, 224512 (2009).